ACS Photonics

Article

pubs.acs.org/journal/apchd5

Multistate Blinking and Scaling of Recombination Rates in Individual Silica-Coated CdSe/CdS Nanocrystals

Siddharth Sampat,[†] Niladri S. Karan,[‡] Tianle Guo,[†] Han Htoon,[‡] Jennifer A. Hollingsworth,[‡] and Anton V. Malko*[,†]

[†]Department of Physics, The University of Texas at Dallas, Richardson, Texas 75080, United States

[‡]Materials Physics & Applications: Center for Integrated Nanotechnologies, Los Alamos National Laboratory, Los Alamos, New Mexico 87545, United States

Supporting Information

ABSTRACT: Nonradiative Auger recombination is the primary exciton loss mechanism in colloidal nanocrystals and an impediment for prospective optoelectronic applications. Recent development of new core/shell nanocrystals with suppressed Auger recombination rates has opened the possibility for studying multicarrier states using time-resolved photoluminescence (PL) spectroscopy. An important aspect not addressed in previous works is the scaling of radiative and nonradiative decay rates with the increasing number and type of excitons in individual nanocrystals. Here we conduct extensive single-dot PL spectroscopy of emissive states in PL blinking trajectories of giant silica-coated CdSe/CdS nanocrystals. At low fluences, we observe the appearance of neutral and charged exciton (trion) states. Both negative and positive trions show strongly suppressed Auger recombination rates resulting in PL quantum yields close to 50%. At higher excitation powers, we observe consecutive emergence of lower efficiency states, indicative of higher order excitons. We employ a scaling model for Auger and radiative decay rates and attribute these states to doubly charged excitons, biexcitons, and a triexciton. Simultaneous analysis of the second-order correlation statistics proves that the biexciton Auger recombination channel can be represented in terms of the superposition of independent recombination channels of trions. Analysis of the PL emission of the triexciton state suggests nonstatistical scaling, likely due to the involvement of the transitions between different symmetries. Finally, measurements at high excitation fluence of nanocrystals with low trion quantum yields does not reveal any higher order excitonic states, corroborating the validity of the scaling model and confirming Auger-related mechanisms responsible for blinking behavior in such core/shell nanocrystals.

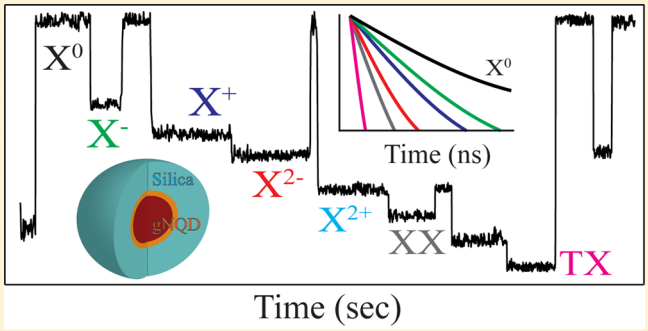

KEYWORDS: *blinking, semiconductor nanocrystals, single-dot spectroscopy, Auger recombination, multiexcitons*

Semiconductor nanocrystal quantum dots (NQDs) have long demonstrated broad technological potential for various optoelectronics applications, ranging from lasers[1] and light-emitting devices[2,3] to biological imaging and molecule tagging[4] to quantum cryptography and communications.[5,6] Among various intrinsic and extrinsic electronic processes found in NQDs, nonradiative Auger recombination plays a central role. In the Auger process, the energy of a recombining electron−hole pair is not converted into a photon, but instead is transferred to a third charge carrier, either an electron or a hole, promoting it to a higher lying energy state. This process is extremely efficient owning to Coulomb interaction of the strongly confined charge particles and relaxation of the momentum conservation requirement. In a large variety of nanocrystals, Auger dynamics range from a few to hundreds of picoseconds,[7] profusely affecting dynamics of multiexcitons and playing a central role in phenomena of fluorescence intermittency ("blinking"). As a result, it severely limits the emissivity of the multicarrier states, complicating realization of lasers and single-photon sources.

Early experiments to study Auger recombination dynamics were conducted via femtosecond transient absorption (TA) measurements in ensemble NQD samples and were primarily focused on the dynamics of the charge neutral multiexcitons.[8,9] They established an important universal trend of Auger lifetimes scaling with the nanocrystal's volume (often referred to as "V-scaling") in a large variety of monocomponent NQDs of various sizes, shapes, and compositions.[7] Scaling of the Auger times with the number of *neutral* excitons N in these nanocrystals has been predicted to follow statistical scaling law that counts the number of possible recombination pathways.[10] A number of experimental studies in ensemble NQD samples has been conducted and reveal a general validity

Received: July 29, 2015
Published: September 25, 2015

DOI: 10.1021/acsphotonics.5b00423
ACS Photonics 2015, 2, 1505−1512

of this rule when applied to symmetric multiexciton configurations. However, the accuracy of these measurements are affected by ensemble inhomogeneity and the majority of data interpretation requires intricate analysis of the femtosecond TA dynamics.[7] More recently, studies of the Auger dynamics of singly charged excitons (trions) have been conducted at the single-nanocrystal level.[11−13] No studies, however, have addressed scaling statistics for higher order charged and neutral multiexcitons at the single-nanocrystal level. Such knowledge, unobscured by ensemble averaging, will likely uncover effects of core/shell composition on photophysical properties and benefit a number of prospective applications.

Recently, a new type of core/shell NQDs in which a CdSe core is overcoated with an especially thick (>10 monolayers) monocrystalline CdS shell has been introduced.[14] These nanocrystals, often dubbed "giant" (gNQDs) due to their larger size (diameters 10−15 nm), possess unique optical properties such as nonblinking PL and strongly suppressed Auger recombination.[15,16] They have shown multiexciton emission in the PL spectra at low temperatures[15] and enhanced biexcitonic emission in ambient conditions, both at the individual nanocrystal level on glass[16,17] and when coupled to the interacting metallic or graphene substrates.[18] Therefore, gNQDs with suppressed Auger recombination present a unique materials system lending themselves to studies of the dynamics of the multiexcitonic states.

In this paper we present, for the first time, a comparative experimental study of the scaling of Auger recombination rates for up to eight different excitonic states conducted on individual nanocrystals. The goal of the study is to evaluate the validity of the multiexciton lifetime scaling and to infer the factors that affect multiexciton recombination dynamics and their influence on the photophysical properties of CdSe/CdS gNQDs. This study has been enabled by a new synthetic approach that allows the fabrication of thick-shell CdSe/CdS gNQDs with an additional silica (SiO_2) coating. This layer facilitates the appearance of a charged exciton and multiexciton states to allow their spectroscopic identification. Photoluminescence blinking traces of individual gNQDs recorded at different excitation powers show the consecutive emergence of several emissive states, each characterized by a well-defined emission intensity and PL lifetime. For low excitation powers we observe emission from neutral exciton (X^0) and singly charged trion states (X^- and X^+), both with suppressed Auger rates. At the higher excitation powers (for the same gNQD), a large variety of additional emissive levels are observed. These discrete and well-defined emissive states are characterized by lower emission quantum yields (QY) and faster PL lifetimes, indicative of higher order excitons. We employed a statistical scaling model for Auger and radiative rates based on the experimentally measured values of PL QYs and lifetimes of neutral exciton and trions. Such analysis allowed us to unambiguously assign the additional emissive levels to doubly negatively and positively charged excitons ($X^{2\pm}$), biexciton (XX), charged biexcitons ($XX^{\pm}$), and triexciton (TX). Further analysis of the TX emission statistics indicate that its scaling deviates from statistical due to the e−h pair recombination occurring between states of different symmetry.

EXPERIMENTAL SECTION

In our experiments we study CdSe/CdS gNQDs that consist of a CdSe core with diameter of $d \approx 4$ nm capped with 16 monolayers of CdS, prepared via the SILAR method as originally described in ref 14. As prepared, CdSe/CdS gNQDs are hydrophobic and form stable suspensions in standard nonpolar solvents. To transfer gNQDs to the aqueous phase, a reverse microemulsion technique is applied to add a surface coating of negatively charged silica that affords SiO_2 thicknesses tunable from 10 to 17.5 nm.[19,20] In brief, Igepal CO-520 (0.5 g), cyclohexane (8 mL), and gNQDs in cyclohexane (450 μL of stock solution; optical density at first absorption peak is 0.15) are sonicated in a vial for 10 min. A 100 μL amount of NH_4OH is then added, and the mixture is sonicated to obtain a clear solution. Finally, tetraethyl orthosilicate (80 μL) is added and the vial is closed and stirred vigorously for 48 h. Silica-coated gNQDs are purified by ethanol and redispersed in nanopure water to obtain a final concentration of ∼5 nM.

For single-dot spectroscopy, aqueous gNQDs are dispersed onto a hydrophilic quartz substrate with the surface density on the order of 0.01 per μm^2. The sample is mounted on a translation stage of an optical microscope, and gNQDs are excited at 405 nm with 50 ps pulses through a 100×, 1.2 NA oil-immersion objective that is also used to collect PL. The interpulse duration is set to be much longer than the PL decay times in order to ensure complete relaxation of excitons between sequential laser pulses. PL signal is sent to a pair of PerkinElmer avalanche photodiodes (SPCM AQR-13) positioned at two arms of the standard Hanbury−Brown−Twiss arrangement with a 50/50 beam splitter. For PL blinking traces only one of the detectors is used, while for biexcitonic quantum yield measurements, second-order photon correlation functions ($g^2(\tau)$) are recorded. Time-tagged time-correlated single-photon counting (TCSPC) is performed using PicoQuant TimeHarp electronics. TCSPC simultaneously records photon arrival times with respect to the beginning of the measurement cycle and to the excitation laser pulse. Hence, it allows us to compile PL decay curves for any particular time segment of the PL intensity trajectory or a chosen window of the intensity distribution function. The overall system time resolution was <1 ns.

RESULTS AND DISCUSSION

The simplest electron−hole configuration that can be found in a photoexcited nanocrystal is a neutral exciton, X^0, followed by singly charged excitonic states, trions ($X^{\pm}$). The negative trion (X^-) consists of two electrons in the $1S_e$ state and a hole in $1S_h$ state, while the positive trion (X^+) has a reversed order, one electron and two holes (Figure 1b). In principle, for NQDs with strongly suppressed Auger rates, more emissive states corresponding to higher order excitons are expected. When a nanocrystal is consecutively charged with additional electrons and holes, we expect the emergence of doubly charged trions (X^{2-} and X^{2+}), Figure 1b. At higher excitation levels, when direct photogeneration of biexcitons is possible, extra charging is expected to result in charged biexcitons, XX^- and XX^+, Figure 1c, and subsequently, a neutral triexciton (TX, three electrons and three holes).

One of the mechanisms that may produce singly and doubly charged excitons is electron injection from nearby impurities. It is a well-known effect in epitaxial QDs grown on the wetting layer where impurities in the surrounding solid-state matrix serve as charge donors or acceptors. Epitaxially grown QDs normally exhibit smaller Auger rates, resulting in the appearance of multiply charged excitonic states in the PL emission spectra.[21] As we have previously reported,[20] the SiO_2

DOI: 10.1021/acsphotonics.5b00423
ACS Photonics 2015, 2, 1505−1512

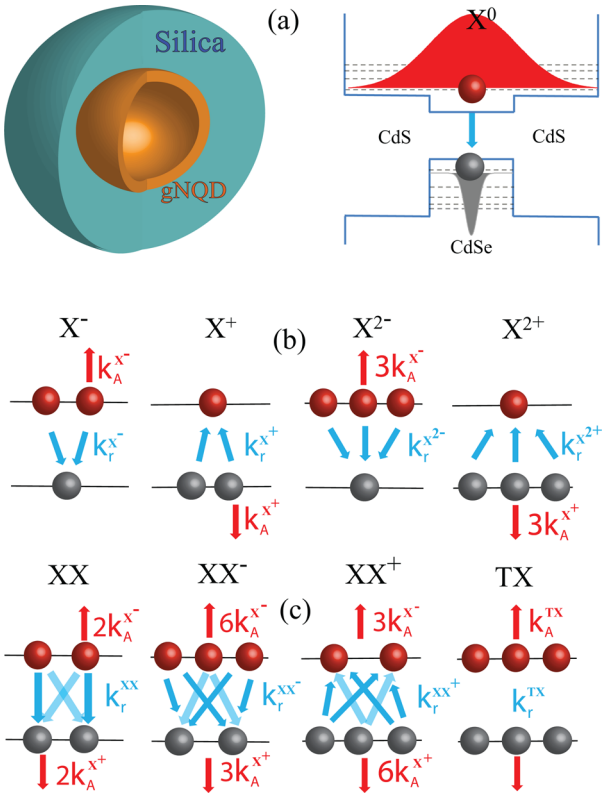

Figure 1. (a) Schematics of silica-coated gNQD and localization of an electron and a hole in a gNQD. Schematics of (b) singly and doubly charged excitons and (c) neutral and charged biexcitons and triexciton. Blue arrows show possible radiative recombination pathways with the total radiative rate for each type of exciton. Red arrows show total Auger recombination rate in units of singly charged trion Auger rates as described in the equations in the text.

shell that encapsulates gNQD is a mesoporous layer rather than a solid, crystalline one. Likely, the hydrolysis or polymerization of the starting tetraethyl orthosilicate (TEOS) is incomplete and results in the porous nature of this shell. We suggest that lone pair electrons on the oxygen atoms of the sol–gel siloxane bonds may serve as electron-donating sites adding to the photogenerated charge carriers in the gNQD. In our recent work,[20] we observed PL emission from various types of SiO_2-coated gNQDs to show either quenched or quasi-stable or "flickering" emission. A quasi-continuous distribution of the emissive states has previously been observed in some medium-sized CdSe/CdS gNQDs[22] and can be a result of the fast switching between multiply charged states on time scales shorter than the binning time of the TCSPC measurement, as shown in Figure S1 (Supporting Information).

In this work, a subset of gNQDs coated with a 17 nm silica shell exhibits a markedly different blinking behavior, with the appearance of a large number of discrete and separable emission levels. Figure 2 displays the PL intensity trajectory, corresponding intensity histogram, and decay dynamics for such a dot at a low pump fluence of N_{av} = 0.2 pair per pulse to avoid direct generation of multiexcitons. The highest intensity level corresponding to peak #1 in the PL histogram (red-shaded region) can be ascribed to a fully "bright", neutral exciton emission. The next two peaks in the histogram (#2 and #3) are attributed to partially emissive, "gray" states from negatively (X^-) and positively (X^+) charged excitons.[13,23] The PL intensity levels of charged states are dictated by the degree of Auger recombination for the corresponding three-particle recombination channel. It was shown earlier that Auger recombination of X^- in CdSe/CdS gNQDs can be completely suppressed,[12] resulting in apparent "blinking-free" behavior. On the other hand, the Auger rate for X^+ is usually larger than that of negative trions ($k_A^{X+} \gg k_A^{X-}$),[24] with the maximum observed quantum yields $QY(X^+) \approx 5\%$.[13] This asymmetric behavior is, in part, a consequence of the greater density of the valence band states and more pronounced hole localization in the gNQD's core as compared to that of an electron, which tends to delocalize over a much larger volume of the gNQD.

In the past, it was widely assumed that radiative times in the core/shell nanocrystals scale statistically, implying linear superposition of the decay channels.[25] In the case of trions ($X^{\pm}$), this assumption leads to their radiative decay times being twice as short as that of the neutral exciton, i.e., $\tau_r^X/\tau_r^{X^{\pm}} = \beta_{stat} = 2$. However, given the quasi-type-II confinement in CdSe/CdS gNQDs, the Coulomb potential of the core-localized hole confines the electron closer to the core. An additional electron introduced to the gNQD (as in X^-) would now experience a repulsion from the core due to the presence of the core-bound electron, effectively "shielding" Coulomb attraction of the hole. Both electrons would also tend to repel each other, causing further reduction in the electron–hole overlap. As a result, β (overlap factor) will be smaller than the ideal value of $\beta = 2$. Recently, the measurements obtained for the intentionally alloyed CdSe/CdS gNQDs have shown β in the range 1.5–1.7.[13] On the contrary, we do not expect a significant reduction of β for X^+. The valence band offsets in these CdSe/CdS gNQDs are much larger (~0.4 eV), leading to the strong localization of both holes in the core regardless of the much smaller Coulomb repulsion.

We now analyze PL intensity levels and decay traces extracted from the color coding for these states as shown in

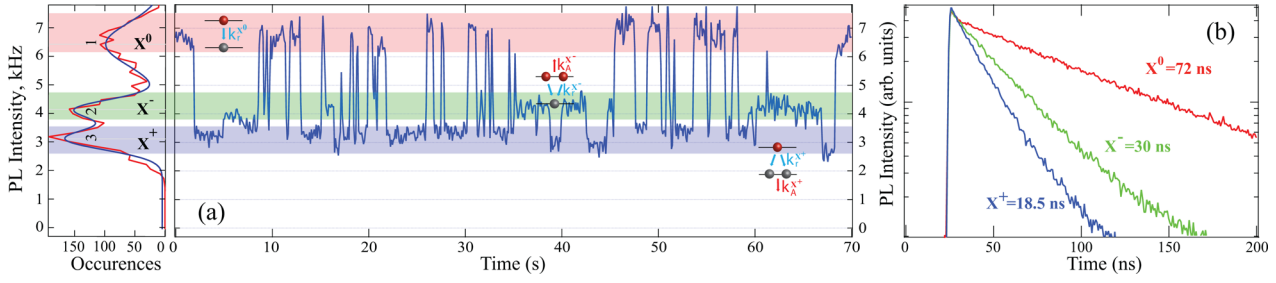

Figure 2. (a) PL intensity histogram and PL blinking trace and (b) extracted PL lifetime traces color coded to three intensity levels shown in (a). Excitation level $N_{av} \approx 0.2$.

DOI: 10.1021/acsphotonics.5b00423
ACS Photonics 2015, 2, 1505–1512

Figure 2. A certain PL intensity level I_i can be ascribed to each of the states, and the experimentally measured PL quantum yield (QY^i) is given by the ratio of the intensity of the state to the intensity of X^0: $QY^i = I_i/I_{X^0}$ assuming that $QY(X^0) = 1$.[16] Using the PL intensity histogram to obtain average values of intensities of each of the emissive states, we find $QY(X^-) = 0.62$ and $QY(X^+) = 0.48$. High values of the $X^\pm$ quantum yields imply that for these species Auger rates are comparable to radiative decay rates. Exponential fits to PL decays yield the lifetimes $\tau^{X^0} = 72$ ns, $\tau^{X^-} = 30$ ns, and $\tau^{X^+} = 18.5$ ns. The radiative decay rate k_r^i of a charged state "i" can be related to the decay rate of the neutral exciton, $k_r^{X^0}$, as in eq 1,

$$k_r^i = \beta^i k_r^{X^0} \tag{1}$$

while the quantum yield of a charged state "i" in the presence of a nonradiative Auger process is defined as shown in eq 2:

$$QY^i = \frac{k_r^i}{k_r^i + k_A^i} \tag{2}$$

where k_A^i is Auger decay rate of this state.

As a result, the following expressions relate Auger rates of the trions, experimentally measured quantum yields, $QY^{X^\pm}$, measured PL lifetimes, $\tau^{X^\pm}$, and β factors.

$$\beta^{X^\pm} = \frac{QY^{X^\pm}\tau_r^{X^0}}{\tau^{X^\pm}} \tag{3a}$$

$$k_A^{X^\pm} = k_r^{X^\pm}\left(\frac{1}{QY^{X^\pm}} - 1\right) \tag{3b}$$

$$\frac{1}{\tau^{X^\pm}} = k^{X\pm} = k_r^{X^\pm} + k_A^{X^\pm} \tag{3c}$$

Using the measured values of quantum yields, lifetimes of $X^\pm$ and $\tau_r^{X^0} = 72$ ns, we extract $\beta^{X^-} = 1.49$ and $\beta^{X^+} = 1.87$, in close agreement with previous measurements.[13] Next, we evaluate scaling of the radiative and Auger recombination rates for multiply charged species. As described earlier, the radiative scaling factor β^i depends on the number of extra electrons or holes present in the gNQD core and may differ considerably from the ideal scaling law. It has been recently shown[26] that radiative and Auger rates for excitonic species charged with extra numbers of electrons ($-\delta$) or holes ($+\delta$) are given by

$$k_r^{X\pm\delta} = \beta^{X\pm\delta} k_r^{X^0} \tag{4a}$$

$$k_A^{X\pm\delta} = \frac{\delta(\delta+1)}{2} k_A^{X^\pm} \tag{4b}$$

In the case of statistical scaling, $\beta_{stat} = 1 + \delta$ regardless of the sign of the extra added charge. Similarly, scaling of radiative and Auger rates for neutral and charged biexcitonic species can be written as

$$k_r^{XX\pm\delta} = \beta^{XX\pm\delta} k_r^{X^0} \tag{5a}$$

$$k_A^{XX\pm\delta} = (1+\delta)(2+\delta)k_A^{X^\pm} + (2+\delta)k_A^{X^\mp} \tag{5b}$$

$$k_A^{XX} = 2(k_A^{X^-} + k_A^{X^+}) \tag{5c}$$

Here, ideally $\beta_{stat} = 2(2 + \delta)$. As expected, Auger decay rates of multiexcitonic species are directly related to those of trions that represent an elementary three-particle Auger recombination channel.[26]

At this moment, we would like to point out that the above application of the statistical model is valid only when applied to the recombination involving states of the same symmetries. In CdSe-based nanocrystals, a third electron or hole will necessarily occupy the 1P state. However, the hole's energy levels are split due to the effects of exchange interactions, internal crystal field, and shape anisotropy.[27] At room temperature, the S and P states of the hole are thermally mixed, resulting in a quasi-continuum of the states. As a result, it is expected that an electron in the P state will be able to recombine with any hole and thus follow statistical scaling.[28]

Following statistical scaling, we considered β factors for a number of excitonic complexes. We expect that due to the quasi-type-II confinement found in CdSe/CdS gNQDs, β is close to ideal for positively charged species (as for X^{2+}) due to the tight confinement of the holes, but may be considerably smaller for negatively charged ones (as for X^{2-}). In case of the neutral biexciton (XX), $\beta = 4$; however, taking into account electron delocalization, a more representative figure is estimated as $\beta^{XX} \approx (\beta^{X^-} + \beta^{X^+}) \approx 3.4$. Table 1 summarizes ideal and expected values of β, where values for X^+ and X^- are calculated from the experiment. In our later analysis, we discuss the effect of variations in values of β on the identification of the emissive states.

Table 1. β Factors

state	statistical scaling	expected scaling
X^-	2	1.49 (measured)
X^+	2	1.87 (measured)
X^{2-}	3	2 (expected)
X^{2+}	3	3 (expected)
XX	4	3.4 (measured)
XX^-	6	5 (expected)
XX^+	6	6 (expected)

To observe signatures of the multiexcitons and higher order charged exciton states in the PL emission, we recorded PL blinking data at a higher excitation level of $N_{av} \approx 1.4$, as seen in Figure 3. In addition to the previously observed states (labeled #1, #2, and #3) with PL lifetimes corresponding to the previously identified X^0 and $X^\pm$ states, several additional states can now be resolved. Their lower PL quantum yields and faster PL lifetimes suggest higher order excitonic states.

Using eqs 3, 4, and 5, together with expected values of β and Auger rates $k_A^{X^\pm}$ of trions as the input parameters, we can compute expected values of quantum yields and PL lifetimes for various types of excitons. We then compare them with the experimentally observed quantum yields $QY_i = I_i/I_{X^0}$ and PL lifetimes that are shown in Figure 3 for the newly emerging states #4–6 in the PL intensity histogram. It is seen that unlike X^0 and $X^\pm$ states, which are unmistakably separable (peaks #1–3 in the histogram), states #4–6 in the lower intensity region appear to be more ambiguous and overlap considerably. One possible reason for this behavior is fast switching between the states on the time scale shorter than the binning time (20 ms), resulting in the appearance of "flickering" behavior. Nonetheless, detailed analysis of the blinking trace reveals a larger

DOI: 10.1021/acsphotonics.5b00423
ACS Photonics 2015, 2, 1505–1512

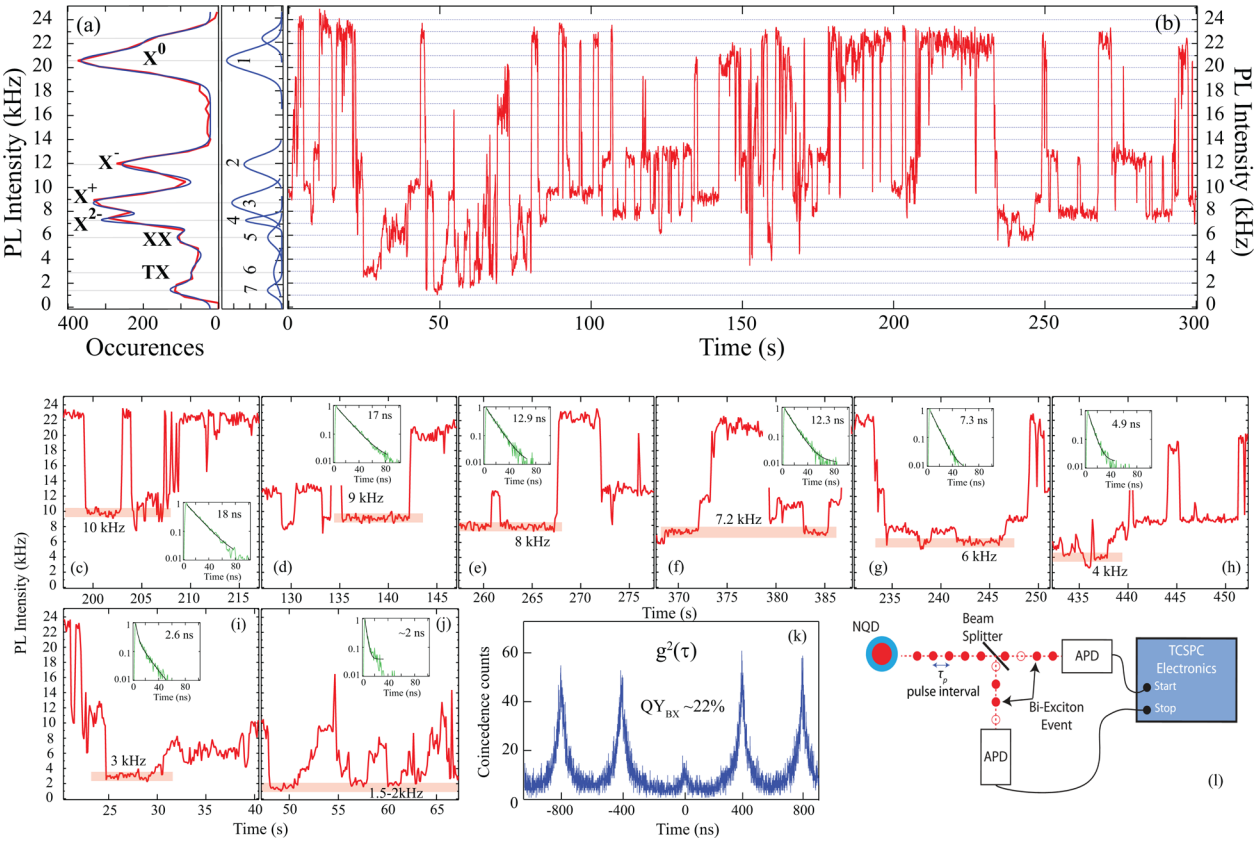

Figure 3. (a) PL intensity histogram and (b) PL blinking trace of the same silica-coated gNQD at the excitation level $N_{av} \approx 1.4$. (c–j) Expanded view of the blinking trace at certain time intervals illustrating the number of distinct intensity levels. Insets: PL lifetimes extracted for the duration of each intensity level as indicated by the shaded regions. (k) Second-order correlation function $g^2(\tau)$ for this particular gNQD. (l) Schematics of the two-photon correlation setup for direct measurements of biexciton quantum yield.

Table 2. Comparison of the Experimentally Measured PL QYs and PL Lifetimes of Multicharged States with Their Computed Values Using Equations in the Text[a]

peak no.	PL counts (kHz)	measd $QY_i = I_i/I_{X^0}$	measd τ_m (ns)	β	computed QY_c	computed τ_c(ns)	assigned state
1	21	1.00	68.0				X^0
2	12	0.57	27	1.49	0.57	26.1	X^-
3	10	0.48	18	1.87	0.48	17.3	X^+
3	9	0.43	17	1.87	0.43	15.6	X^+
3	8	0.38	12.9	2	0.37	12.7	X^{2-}
4	7.2	0.34	12.3	2	0.37	12.7	X^{2-}
5	6	0.29	7.3	3–3.4	0.22	7.0	X^{2+} and XX
6	4	0.19	4.9	5–6	0.27	3	$XX^{\pm}$
6	3	0.14	2.6	7–8	0.18	1.7	TX
7	1.5	0.07	2				dark

[a]Assignment of the states is based on comparison of these values. Assignment of the $X^{\pm}$ states is confirmed using previously extracted β values as discussed in the text. *TX* values are shown for the statistical scaling case.

number of separable emission levels than the peaks in the intensity histogram suggest. Panels c–j in Figure 3 show eight separable emission levels below the X^- (I_{X^-} = 12 kHz) emission state. The noise level is discernibly smaller than the separation between the levels, allowing for their individual analysis. PL decay traces are extracted within the duration of each intensity level (shaded regions) and are shown as insets to each of the panels c–j.

Table 2 lists measured PL QYs and lifetimes for the intensity levels shown in Figure 3, compares them to the computed values QY_c and τ_c for several excitonic complexes, and makes assignments of the emissive states. For example, levels at 10, 9, and 8 kHz PL emission intensity are found within the envelope of the X^+ peak in the PL intensity histogram. However, while levels 10 and 9 kHz exhibit similar lifetimes (18 and 17 ns) and match well to the computed parameters of the X^+ state, the 8 kHz level exhibits a 13 ns lifetime, suggesting a different origin. Our analysis shows that levels 8 and 7.2 kHz correspond to doubly negatively charged exciton X^{2-}. It is interesting to note that many states, including the neutral exciton level X^0, are split, as seen in Figures 2 and 3. It is possibly a result of the modified charging environment due to the presence of the silica shell. Peak #5 (at I_i = 6 kHz) corresponds to PL parameters of a neutral biexciton, *XX*. At the same time, calculations also

DOI: 10.1021/acsphotonics.5b00423
ACS Photonics 2015, 2, 1505–1512

suggest that the doubly positively charged exciton, X^{2+}, has similar computed parameters ($QY_c^{X^{2+}} = 0.28$ and $\tau_c^{X^{2+}} = 6.5$ ns). However, we argue that this emission more likely originates from biexcitonic recombination. The intensity level of 4 kHz remains largely unidentified, possibly originating from charged biexcitons ($XX^{\pm}$).

Direct measurements of multiexciton dynamics in single nanocrystals at ambient temperatures are often challenging due to the low emission quantum yield of these species and superposition of the emission lines in the PL spectrum. Nevertheless, direct measurements of the biexciton dynamics[13,29,30] indicate that the rate of the Auger recombination can indeed be presented as the superposition of the independent negative and positive trion pathway as written in eqs 5. Taking into account scaling of the radiative recombination rate k_r^{XX}, we compute XX PL emission quantum yield and lifetime as shown in Table 2. These values are close to the measured QY and PL lifetimes of peak #5 in the PL histogram in Figure 3. Furthermore, the biexciton quantum yield QY^{XX} can be independently measured via two-photon correlation statistics as was recently shown.[16,31] Panel k in Figure 3 presents the normalized second-order correlation function $g^2(\tau)$. The value of $g^2(0) = QY^{XX} \approx 0.22$ is determined from the area ratio of the center and side peaks. As illustrated in the schematics shown in panel l, in the pulsed two-photon correlation experiment only consecutive emission of two photons in quick succession ($XX \rightarrow X \rightarrow 0$) will contribute to the nonzero value of $g^2(0)$. Emission from the X^{2+} state, however, provides only one photon and does not contribute to $g^2(0)$. We therefore conclude that the majority of the emission at the 6 kHz intensity level (peak position #5) represents biexcitonic emission, with possibly some contribution from X^{2+}, as indicated by the difference in quantum yield measurements.

To further test the validity of our approach, we analyze gNQDs with low QY^{XX} that will indicate higher Auger rates for charged excitons. Recently, Vaxenburg et al. have calculated strong dependence of the Auger rates of the X^- excitons in colloidal nanocrystals as a function of their size.[32] Thus, gNQDs with low QY^{XX} are expected in an ensemble due to the inherent size dispersion in the gNQD fabrication process.[33] In such dots, we do not expect to observe the same multitude of the intensity levels at high excitation fluences, as they necessarily will have very low quantum yields. Blinking traces for one such dot from the same ensemble with $QY^{XX} \approx 0.05$ is shown in Figure S2 (Supporting Information). Even at high excitation level $N_{av} \approx 2.6$, only three clear states are observed in the PL intensity histogram. They are similarly ascribed to neutral and charged excitons with measured lifetimes $\tau_{X^0} = 41$ ns, $\tau_{X^-} = 9$ ns, and $\tau_{X^+} = 5.5$ ns and $QY^{X^-} = 0.38$ and $QY^{X^+} = 0.24$, matching the calculated lifetimes. The expected biexciton PL lifetime is calculated to be $\tau_c^{XX} < 2$ ns. No other well-defined intensity levels are observed below the X^+ level, indicating that all multicharged species have even lower QYs and lifetimes.

In addition to various single and charged exciton and biexciton species, peak #6 (3 kHz intensity level) has been assigned to a triexciton, TX. The spectral signatures of TX emission in single CdSe nanocrystals have recently been reported using fast gated PL detection via a streak camera.[30] In that work, the quantum yield of TX emission was estimated to be less than 1% due to strong Auger recombination common for regular NQDs. In the case of gNQD with electron delocalization into the shell, the 1P electron energy level is expected to be only moderately higher as compared to the 1S state due to much larger total gNQD size. This makes it difficult to observe a higher energy shoulder in the integrated PL emission spectra at room temperature. Following the earlier argument about hole's S−P mixing, it is not clear what kind of scaling is expected for TX Auger rates. Neglecting S−P interband transitions and applying selection rules for the optical transitions (so-called "quantum scaling"), Rupasov et al.[10] have theoretically shown the TX Auger time to be 2.5 times smaller than the Auger time of the biexciton, $\tau_A^{XX}/\tau_A^{TX} = 2.5$. Ensemble data extracted from the analysis of the 1S transient absorption dynamics of regular NQDs indicate that τ_A^{XX}/τ_A^{TX} varies from ∼2.3 to ∼3.4 depending on the size of the NQD.[25] On the other hand, statistical scaling of the TX Auger times would lead to a factor of 4.5 difference.[10] For the case of statistical scaling, we would obtain computed $QY_c^{TX} \approx 0.18$ and $\tau_c^{TX} \approx 1.7$ ns (data shown in Table 2), while for quantum scaling, $QY_c^{TX} \approx 0.22$ and $\tau_c^{TX} \approx 3$ ns. Overall, these lifetime values are much lower than those of XX and come close to the measured values only for peak #6 as compared in Table 2. Its fairly low occurrence in the PL distribution histogram as compared to XX further supports its assignment as the TX state. The measured time, $\tau_m^{TX} \approx 2.6$ ns, is substantially different from the predicted value based on the statistical model and may indicate that S−P mixing is not quite complete. Finally, peak #7 can be ascribed to an even higher order charged excitonic complex, with nearly completely quenched "dark" state emission.

It is important to analyze the robustness of the results with respect to variations in the values of β and Auger rates. As discussed, Auger scaling equations for higher order excitons rely on the Auger rates of trions and on the accurate assessment of β factors. As shown in Table 1, β factors for higher order negatively charged excitons, such X^{2-} and XX^-, differ from ideal scaling due to electron delocalization and reduced overlap. However, for higher order excitons Auger rates become prevalent and, for the most part, define the emission from states with low quantum yields. For example, if we consider $\beta = 2.5$ for the X^{2-} state, the computed quantum yield and lifetime parameters would be $QY_c = 0.42$ and $\tau_c = 11.5$ ns, still allowing us to assign peak #4 to this state.

Substantiation of these results within the rate scaling model also has important implications in the context of fluorescence blinking. As described in a recent review,[34] the majority of recent approaches explaining blinking mechanisms fall into two general categories. One approach assumes that charge trapping leaves the nanocrystal core effectively charged, and Auger recombination then nonradiatively quenches the fluorescence of the charged exciton. The other approach assumes that externally trapped charge can quickly (before the next excitation cycle) recombine with its countercharge in the core via some nonradiative mechanism, also resulting in flourescence quenching. In this case, dynamics of the blinking states are determined by the fluctuation of the charging rates. Depending on the materials systems and excitation conditions,[35] there exist experimental data in support of either blinking mechanism. The observation of the multitude of the well-defined emission states with the PL parameters that follow scaling statistics of the recombination rates clearly advocates for the Auger-related origin of blinking in core/shell CdSe/CdS gNQDs.

CONCLUSION

In summary, we performed extensive single-dot spectroscopy studies of the charged and neutral excitons and multiexcitons in

DOI: 10.1021/acsphotonics.5b00423
ACS Photonics 2015, 2, 1505−1512

giant silica-coated CdSe/CdS nanocrystals. Upon the increase of the excitation fluence, we observed the consecutive emergence of up to eight well-defined intensity levels with progressively lower QYs in PL blinking trajectories. Using a scaling approach to describe the evolution of the Auger and radiative recombination rates, we assigned these emission levels to singly and doubly charged exciton, biexciton, and triexciton states. Using PL intensity and second-order correlation function measurements, we confirmed the Auger rate of the biexciton to be twice the sum of the X^- and X^+ Auger decay rates, further proving its decay in terms of a superposition of independent negative and positive trion Auger pathways. PL QY of the triexciton state was found to be ∼14%, the highest reported in the literature. Our studies, performed at the single-nanocrystal level and free from the inhomogeneity effects inherent to ensemble measurements, generally proves the validity of the statistical scaling model for Auger and radiative recombination rates for the lower order excitons. We, however, observed deviations from statistical scaling for triexciton recombination rates, most likely due to transitions involving states with different symmetries. The observation and analysis of highly emissive multiexcitonic complexes will foster future research in the area of colloidal nanostructures with suppressed Auger recombination. We expect such nanoemitters to find numerous applications in areas from biological labeling and imaging to optoelectronics and quantum information.

■ ASSOCIATED CONTENT

Supporting Information

The Supporting Information is available free of charge on the ACS Publications website at DOI: 10.1021/acsphotonics.5b00423.

Illustration of the quasi-stable, "flickering" emission shown by the majority of gNQDs coated with a 12 or 17 nm layer of silica; photon statistics and blinking behavior for the silica-coated gNQD with a low trion and biexciton quantum yield; table of the extracted radiative and Auger lifetimes for each of the excitonic complexes discussed in the main text (PDF)

■ AUTHOR INFORMATION

Corresponding Author

*E-mail: anton.malko@utdallas.edu.

Notes

The authors declare no competing financial interest.

■ ACKNOWLEDGMENTS

Optical studies of single nanocrystals were performed by the UT Dallas group (S.S., T.G., and A.V.M.) and supported by the Department of Energy, Basic Energy Science (DOE/BES), grant DE-SC0010697. Synthesis of the silica-coated giant nanocrystals was performed by the LANL group (N.S.K, J.A.H., and H.H.) and primarily supported by a Division of Materials Science and Engineering DOE, OBES grant (2009LANL1096) for g-NQD development. Work was performed in part at the Center for Integrated Nanotechnologies, a U.S. Department of Energy (DOE), Office of Basic Energy Sciences (OBES) Nanoscale Science Research Center & User Facility, under User Project U2013A0134.

■ REFERENCES

(1) Klimov, V. I.; Mikhailovsky, A. A.; Xu, S.; Malko, A.; Hollingsworth, J. A.; Leatherdale, C. A.; Eisler, H.-J.; Bawendi, M. G. Optical Gain and Stimulated Emission in Nanocrystal Quantum Dots. *Science* **2000**, *290*, 314−317.

(2) Colvin, V. L.; Schlamp, M. C.; Alivisatos, A. P. Light-Emitting Diodes Made From Cadmium Selenide Nanocrystals and a Semiconducting Polymer. *Nature* **1994**, *370*, 354−357.

(3) Caruge, J. M.; Halpert, J. E.; Wood, V.; Bulovic, V.; Bawendi, M. G. Colloidal Quantum-Dot Light-Emitting Diodes with Metal-Oxide Charge Transport Layers. *Nat. Photonics* **2008**, *2*, 247−250.

(4) Bruchez, M. P.; Moronne, M.; Gin, P.; Weiss, S.; Alivisatos, A. P. Semiconductor Nanocrystals as Fluorescent Bilological Labels. *Science* **1998**, *281*, 2013−2016.

(5) Lounis, B.; Bechtel, H. A.; Gerion, D.; Alivisatos, A. P.; Moerner, W. E. Photon Antibunching in Single CdSe/ZnS Quantum Dot Fluorescence. *Chem. Phys. Lett.* **2000**, *329*, 399−404.

(6) Michler, P.; Imamoglu, A.; Mason, M. D.; Carson, P. J.; Strouse, G. F.; Buratto, S. K. Quantum Correlation Among Photons from a Single Quantum Dot at Room Temparature. *Nature* **2000**, *406*, 968−970.

(7) Robel, I.; Gresback, R.; Kortshagen, U.; Schaller, R. D.; Klimov, V. I. Universal Size Dependent Trend in Auger Recombination in Direct-Gap and Indirect-Gap Semiconductor Nanocrystals. *Phys. Rev. Lett.* **2009**, *102*, 177404.

(8) Klimov, V. I.; Mikhailovsky, A. A.; McBranch, D. W.; Leatherdale, C. A.; Bawendi, M. G. Quantization of Multiparticle Auger Rates in Semiconductor Quantum Dots. *Science* **2000**, *287*, 1011−1013.

(9) Pandey, A.; Guyot-Sionnest, P. Multicarrier Recombination in Colloidal Quantum Dots. *J. Chem. Phys.* **2007**, *127*, 111104.

(10) Klimov, V. I.; McGuire, J. A.; Schaller, R. D.; Rupasov, V. I. Scaling of Multiexciton Lifetimes in Semiconductor Nanocrystals. *Phys. Rev. B: Condens. Matter Mater. Phys.* **2008**, *77*, 195324−1/12.

(11) Galland, C.; Ghosh, Y.; Steinbrück, A.; Sykora, M.; Hollingsworth, J. A.; Klimov, V. I.; Htoon, H. Two types of Luminescence Blinking Revealed by Spectroelectrochemistry of Single Quantum Dots. *Nature* **2011**, *479*, 203−207.

(12) Galland, C.; Ghosh, Y.; Steinbrück, A.; Hollingsworth, J. A.; Htoon, H.; Klimov, V. I. Lifetime Blinking in Nonblinking Nanocrystal Quantum Dots. *Nat. Commun.* **2012**, *3*, 908.

(13) Park, Y.-S.; Bae, W. K.; Pietryga, J. M.; Klimov, V. I. Auger Recombination of Biexcitons and Negative and Positive Trions in Individual Quantum Dots. *ACS Nano* **2014**, *8*, 7288−7296.

(14) Chen, Y.; Vela, J.; Htoon, H.; Casson, J. L.; Werder, D. J.; Bussian, D. A.; Klimov, V. I.; Hollingsworth, J. A. Giant" Multishell CdSe Nanocrystal Quantum Dots with Suppressed Blinking. *J. Am. Chem. Soc.* **2008**, *130*, 5026−5027.

(15) Htoon, H.; Malko, A. V.; Bussian, D.; Vela, J.; Hollingsworth, J. A.; Chen, Y.; Klimov, V. I. Highly Emissive Multiexcitons in Steady-State Photoluminescence of Individual "Giant" CdSe/CdS Core/Shell Nanocrystals. *Nano Lett.* **2010**, *10*, 2401−2407.

(16) Park, Y.-S.; Malko, A. V.; Vela, J.; Ghosh, Y.; Garcia-Santamaria, F.; Hollingsworth, J. A.; Klimov, V. I.; Htoon, H. Near-Unity Quantum Yields of Biexciton Emission from CdSe/CdS Nanocrystals Measured Using Single-Particle Spectroscopy. *Phys. Rev. Lett.* **2011**, *106*, 187401/1−4.

(17) Mangum, B. D.; Sampat, S.; Ghosh, Y.; Hollingsworth, J. A.; Htoon, H.; Malko, A. V. Influence of the Core Size on Biexciton Quantum Yield of Giant CdSe/CdS Nanocrystals. *Nanoscale* **2014**, *6*, 3712−3720.

(18) Park, Y.-S.; Ghosh, Y.; Xu, P.; Mack, N. H.; Wang, H.-L.; Hollingsworth, J. A.; Htoon, H. Single-Nanocrystal Photoluminescence Spectroscopy Studies of Plasmon-Multiexciton Interactions at Low Temperature. *J. Phys. Chem. Lett.* **2013**, *4*, 1465−1470.

(19) Ding, H. L.; Zhang, Y. X.; Wang, S.; Xu, J. M.; Xu, S. C.; Li, G. H. Fe3O4@SiO2 Core/Shell Nanoparticles: The Silica Coating Regulations with a Single Core for Different Core Sizes and Shell Thicknesses. *Chem. Mater.* **2012**, *24*, 4572−4580.

DOI: 10.1021/acsphotonics.5b00423
ACS Photonics 2015, 2, 1505−1512

(20) Karan, N. S.; Keller, A. M.; Sampat, S.; Roslyak, O.; Arefin, A.; Hanson, C. J.; Casson, J. L.; Desireddy, A.; Piryatinski, A.; Iyer, R.; et al. Plasmonic Giant Quantum Dots: Hybrid Semiconductor-Metal Nanostructures for Truly Simultaneous Optical Imaging, Photothermal Effect and Thermometry. *Chem. Sci.* **2015**, *6*, 2224−2236.
(21) Baier, M. H.; Malko, A.; Pelucchi, E.; Oberli, D. Y.; Kapon, E. Quantum Dot Exciton Dynamics Probed by Photon Correlation Spectroscopy. *Phys. Rev. B: Condens. Matter Mater. Phys.* **2006**, *73*, 205321.
(22) Malko, A. V.; Park, Y.-S.; Sampat, S.; Vela, J.; Chen, Y.; Hollingsworth, J. A.; Klimov, V. I.; Htoon, H. Pump-Intensity- and Shell-Thickness-Dependent Evolution of Photoluminescence Blinking in Individual Core/Shell CdSe/CdS Nanocrystals. *Nano Lett.* **2011**, *11*, 5213−5218.
(23) Spinicelli, P.; Buil, S.; Quélin, X.; Mahler, B.; Dubertret, B.; Hermier, J.-P. Bright and Grey States in CdSe-CdS Nanocrystals Exhibiting Strongly Reduced Blinking. *Phys. Rev. Lett.* **2009**, *102*, 136801.
(24) Cragg, G. E.; Efros, A. L. Suppression of Auger Processes in Confined Structures. *Nano Lett.* **2010**, *10*, 313−317.
(25) McGuire, J. A.; Joo, J.; Pietryga, J. M.; Schaller, R. D.; Klimov, V. I. New Aspects of Carrier Multiplication in Semiconductor Nanocrystals. *Acc. Chem. Res.* **2008**, *41*, 1810−1819.
(26) Gao, Y.; Roslyak, O.; Dervishi, E.; Karan, N. S.; Ghosh, Y.; Sheehan, C. J.; Wang, F.; Gupta, G.; Mohite, A.; Dattelbaum, A. M.; et al. Hybrid Graphene-Giant Nanocrystal Quantum Dot Assemblies with Highly Efficient Biexciton Emission. *Adv. Opt. Mater.* **2015**, *3*, 39−43.
(27) Efros, A. L.; Rosen, M. The Electronic Structure of Semiconductor Nanocrystals. *Annu. Rev. Mater. Sci.* **2000**, *30*, 475.
(28) Park, Y.-S.; Ghosh, Y.; Chen, Y.; Piryatinski, A.; Xu, P.; Mack, N. H.; Wang, H.-L.; Klimov, V. I.; Hollingsworth, J. A.; Htoon, H. Super-Poissonian Statistics of Photon Emission from Single CdSe-CdS Core-Shell Nanocrystals Coupled to Metal Nanostructures. *Phys. Rev. Lett.* **2013**, *110*, 117401/1−5.
(29) Jha, P. P.; Guyot-Sionnest, P. Trion Decay in Colloidal Quantum Dots. *ACS Nano* **2009**, *3*, 1011−1015.
(30) Zhao, J.; Nair, G.; Fisher, B. R.; Bawendi, M. G. Challenge to the Charging Model of Semiconductor-Nanocrystal Fluorescence Intermittency from Off-State Quantum Yields and Multiexciton Blinking. *Phys. Rev. Lett.* **2010**, *104*, 157403/1−4.
(31) Nair, G.; Zhao, J.; Bawendi, M. G. Biexciton Quantum Yield of Single Semiconductor Nanocrystals from Photon Statistics. *Nano Lett.* **2011**, *11*, 1136−1140.
(32) Vaxenburg, R.; Rodina, A.; Shabaev, A.; Lifshitz, E.; Efros, A. L. Nonradiative Auger Recombination in Semiconductor Nanocrystals. *Nano Lett.* **2015**, *15*, 2092−8.
(33) Xie, R.; Kolb, U.; Li, J.; Basché, T.; Mews, A. Synthesis and Characterization of Highly Luminescent CdSe-core CdS/Zn0.5Cd0.5S/ZnS Multishell Nanocrystals. *J. Am. Chem. Soc.* **2005**, *127*, 7480−7488.
(34) Cordones, A. A.; Leone, S. R. Mechanisms For Charge Trapping in Single Semiconductor Nanocrystals Probed by Fluorescence Blinking. *Chem. Soc. Rev.* **2013**, *42*, 3209−3221.
(35) Knappenberger, K. L.; Wong, D. B.; Romanyuk, Y. E.; Leone, S. R. Excitation Wavelength Dependence of Fluorescence Intermittency in CdSe/ZnS Core/Shell Quantum Dots. *Nano Lett.* **2007**, *7*, 3869−3874.

DOI: 10.1021/acsphotonics.5b00423
ACS Photonics 2015, 2, 1505−1512